

Characteristic Variables and Entrainment in 3-D Density Currents

S. Hormozi¹, B. Firoozabadi^{1,*} and H. Ghasvari Jahromi¹

A CFD code has been developed to describe the salt solution density current, which propagates three-dimensionally in deep ambient water. The height and width of the dense layer are two dominated length scales in a 3-D structure of the density current. In experimental efforts, it is common to measure the height and width of this current via its brightness. Although there are analytical relations to calculate the current height in a two-dimensional flow, these relations cannot be used to identify the width and height of a 3-D density current, due to the existence of two unknown parameters. In the present model, the height and width of the dense layer are obtained by using the boundary layer concept. Also, a comparison is made between depth averaged and characteristic variables. Then, the computed velocity and concentration profiles are compared with the experimental data and the results show good agreement between them. In this work, the entrainment coefficient was also calculated using depth-averaged parameters and compared with the experimental data. The result has the same trend as the Ellison and Turner experiments. Present results show that the boundary layer concept can be useful in identifying the height and width of a 3-D density current.

INTRODUCTION

Gravity currents, on inclined boundaries, are formed when the inflow fluid has a density difference with the ambient fluid and the tangential component of gravity becomes the driving force. The salinity concentration and/or the temperature differences cause the density differences. Sometimes, the extra weight of suspended solids causes the density difference, for example, in turbidity currents in the ocean or a large lake and in powder snow avalanches in the mountains. The density current is a three-dimensional flow by nature. Important applications of these currents are found in various fields, such as in the protection of seafaring vessels, atmospheric pollution, entomology and pest control, gas compression technology, meteorology and weather forecasting, cleaning of oil spills and the control of sedimentation in reservoirs, etc. When two fluids with different density have a low relative velocity to each other, shear exists across the interface and, initially, the developing flow is laminar. Then, if a critical value of shear is reached, the flow becomes

dynamically unstable and gentle waves begin to form at the interface (crests normal to the shear direction). By increasing the velocity, the wave amplitude continuously grows and eventually reaches the roll-up or breaking point, which is called the Kelvin-Helmholtz wave. Within each wave, there exists some lighter fluid that has been rolled under the denser fluid, resulting in patches of static instability [1] (Figure 1). Static instability combines with continued dynamic instability and causes each wave to become turbulent. Turbulence spreads throughout the layer, causing diffusion or mixing of the different fluids. In this phase, some momentum is transferred between the fluids and the shear between the layers is reduced; the formerly sharp interface becoming broader. In density currents, in laboratory experiments, the interface of two layers is identified by its brightness and by the naked eye, which is based on penetration of the dense layer into the clean lighter fluid. Besides, in analytical research, there are some relations for calculating average height, which was developed, based on two-dimensional flows. Different single value variables have been used for non-dimensionalizing vertical profiles in 2-D density or turbidity currents. However, in three-dimensional flows, the lateral propagation is added to the height of the current, so using analytical relations are not suitable, because those relations do not give any information

1. Department of Mechanical Engineering, Sharif University of Technology, P.O. Box 11155-9567, Tehran, Iran.

*. To whom correspondence should be addressed. E-mail: firoozabadi@sharif.edu

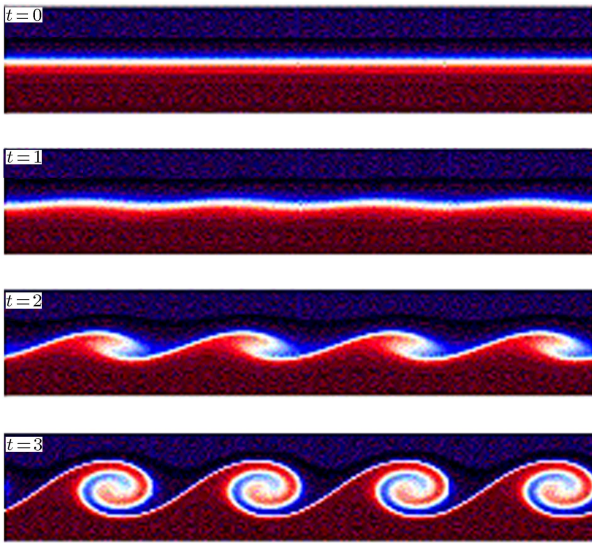


Figure 1. Kelvin-Helmholtz instability formed at the interface of two layers with different densities [1].

regarding the width of the current. In the present model, by computing the height and width of the dense layer, based on the boundary layer concept, the averaged-parameters can be obtained and the entrainment coefficient versus averaged Richardson number is calculated. Much laboratory experimentation and numerical research into density or turbidity currents that studied depth-averaged and characteristic values or entrainment [2-9] were performed in 2-D modeling. Relatively few studies addressing 3-D density currents are available in the literature. Alavian [10] investigated, experimentally, the 3-D behavior of a salt solution density current released down a sloping surface in a tank of fresh water. Observations and measurements have revealed a variety of phenomena depending strongly on buoyancy flux, Richardson number and angle of inclination.

The objective of the present study is to simulate the flow characteristics of a 3-D density current, with individually average parameters and an entrainment coefficient, in a straight inclined channel. Also, a new approach is introduced, based on the boundary layer concept, to obtain the height and lateral propagation of a density current. The entrainment coefficient against Richardson number is obtained without any approximation (Alavian [7] obtained the entrainment coefficient against the approximated normal Richardson number). Also, the water entraining to the dense layer in a span-wise direction is considered, which is neglected in all previous 2-D simulations. An equation, which relates the entrainment coefficient and the Richardson number is introduced and replaced with the previous proposed equations which were 2-D numerical or experimental investigations. Finally, the simulation results of the present study are compared

to the experimental data of Alavian [7], which show reasonable agreement.

MATHEMATICAL MODELING

Governing Equations

Figure 2 shows the schematic sketch of a 3-D density current. Because the density difference is very small, compared to the density of the inflow fluid, density currents caused by saline water are often analyzed by the Boussinesq approximation, in which the relative density difference is only considered in the gravity term but is neglected in other terms in the momentum equation. Due to the low concentration of the salt solution, the fluid could be assumed as Newtonian. The equations, which describe the motion of a density current, can be expressed as:

$$\frac{\partial u}{\partial x} + \frac{\partial v}{\partial y} + \frac{\partial w}{\partial z} = 0, \tag{1}$$

$$u \frac{\partial u}{\partial x} + v \frac{\partial u}{\partial y} + w \frac{\partial u}{\partial z} = -\frac{1}{\rho} \frac{\partial P}{\partial x} + g' \sin \theta + \frac{\partial}{\partial x} \left(v \frac{\partial u}{\partial x} \right) + \frac{\partial}{\partial y} \left(v \frac{\partial u}{\partial y} \right) + \frac{\partial}{\partial z} \left(v \frac{\partial u}{\partial z} \right), \tag{2a}$$

$$u \frac{\partial v}{\partial x} + v \frac{\partial v}{\partial y} + w \frac{\partial v}{\partial z} = -\frac{1}{\rho} \frac{\partial P}{\partial y} - g' \cos \theta + \frac{\partial}{\partial x} \left(v \frac{\partial v}{\partial x} \right) + \frac{\partial}{\partial y} \left(v \frac{\partial v}{\partial y} \right) + \frac{\partial}{\partial z} \left(v \frac{\partial v}{\partial z} \right), \tag{2b}$$

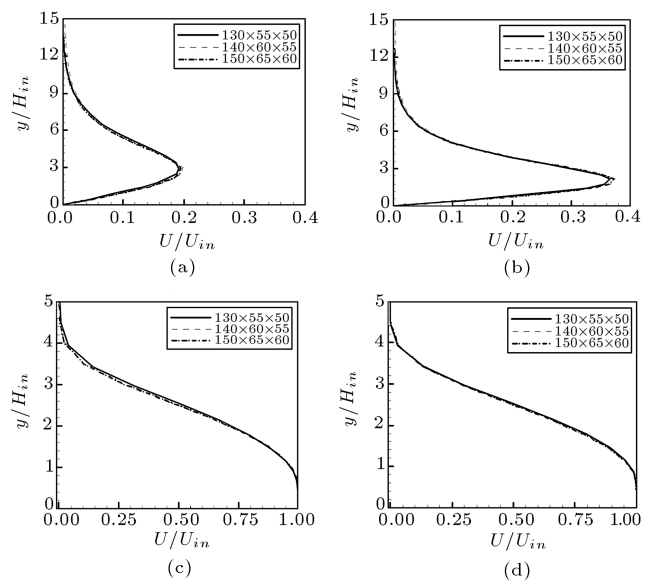


Figure 2. Grid independency; dimensionless velocity profile at a) $x = 2.5$ m and b) $x = 1.5$ m. Dimensionless concentration profile at c) $x = 2.5$ m and d) $x = 2.5$ m.

$$u \frac{\partial w}{\partial x} + v \frac{\partial w}{\partial y} + w \frac{\partial w}{\partial z} = -\frac{1}{\rho} \frac{\partial P}{\partial z} + \frac{\partial}{\partial x} \left(\nu \frac{\partial w}{\partial x} \right) + \frac{\partial}{\partial y} \left(\nu \frac{\partial w}{\partial y} \right) + \frac{\partial}{\partial z} \left(\nu \frac{\partial w}{\partial z} \right), \quad (2c)$$

$$u \frac{\partial C}{\partial x} + v \frac{\partial C}{\partial y} + w \frac{\partial C}{\partial z} = \lambda \left(\frac{\partial^2 C}{\partial x^2} + \frac{\partial^2 C}{\partial y^2} + \frac{\partial^2 C}{\partial z^2} \right). \quad (3)$$

These equations are continuity, momentum and diffusion, respectively. u, v, w are the components of the velocity in x, y and z directions; $g' = g(\rho - \rho_w)/\rho_w$ is the reduced acceleration of gravity; ρ and ρ_w are the density of the saline solution and pure water, respectively and C is the volumetric concentration of the mixture, which is defined as:

$$C = \frac{\rho - \rho_w}{\rho_s - \rho_w}, \quad (4)$$

where ρ_s is the density of the salt, θ is the bed slope and ν and λ are the viscosity and diffusivity of the fluid, respectively. The pressure term, p , denotes instantaneous pressure, which is subtracted from the hydrostatic pressure.

Boundary Conditions

The boundary conditions at the inlet are known. Similar to the Alavian experiments [10], the salt-solution flow with uniform velocity and concentration enters the channel under a still body of water via a sluice gate onto a surface inclined at angle θ . At the outlet boundary, the streamwise gradients of all variables are set to zero. It is expected that the outlet has only a local effect on the flow field [11]. At the free surface, the rigid-lid approximation is made, then, a symmetrical condition is applied that includes zero gradients and zero fluxes perpendicular to the boundary [11]. At the rigid walls, due to the no slip conditions and a pure depositing assumption, the velocities and concentration gradients are set zero. For the concentration equation, zero gradient conditions, normal to the vertical walls and zero-flux conditions, normal to the bottom, are applied.

Solution Procedure

The governing equations are solved by a finite-volume method, using boundary fitted coordinates. The continuity, momentum and diffusion equations are solved for velocity components, u_i , and concentration, C , in fixed Cartesian directions on a non-staggered grid. All the variables are, thus, stored at the center of the control volume. The velocity components at the control volume face are computed by the Rhie-Chow

interpolation method [12] and the pressure-velocity coupling is handled by the SIMPLEC method. The convective terms are treated by the hybrid scheme. TDMA-based algorithms are applied for solving the algebraic equations. The solution procedure is iterative and the computations are terminated when the sums of absolute residuals normalized by the inflow fluxes are below 10^{-4} for all variables. Depending on the inlet velocity and bed slope, around 3000-5000 iterations are required to achieve convergence in the velocity fields. However, for the concentration field, convergence is much quicker. Using the present computer with CPU of 1.8 Gigahertz and 1 Gigabyte of Ram, convergence was achieved after 6 hours. The mesh points are chosen as uniform in the flow direction, but in normal and span-wise directions, the grid points are distributed in a non-uniform manner, with a higher concentration of grids close to the bed surface and symmetry plane. Each control volume contains one node at its center, but the boundary adjacent volumes contain two nodes. The effects of different mesh size on flow characteristics, such as velocity profile and concentration profile, were tested and the mesh independency was obtained. Finally, $150 \times 65 \times 60$ in directions x, y and z was selected (Figure 2).

RESULTS AND DISCUSSIONS

To validate the computer program, the inlet boundary conditions are set as Table 1, similar to the Alavian experiments [10]. Salt solution with uniform velocity and concentration is continuously released from a source of a rectangular cross-section and spreads down an incline in a tank of fresh water (Figure 3). The tank is 1.5 m deep, 1.5 m wide and 3 m long. The inlet height of the density current is 7.5 mm and its width is 4.5 cm.

In the above table, Q_0 is the inlet volumetric flux, B_0 is the buoyancy flux, Ri_0 is the inlet Richardson

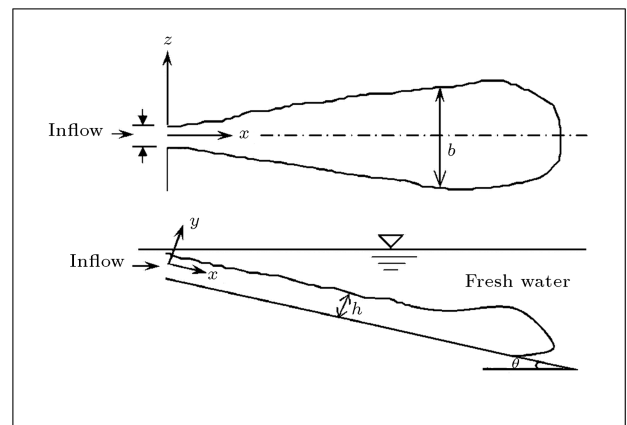


Figure 3. Definition sketch of 3-D density current.

Table 1. The inlet conditions.

Inlet Condition	$\frac{\rho - \rho_w}{\rho_w}$	Q_0 (cm ³ /s)	B_o (cm ⁴ /s ³)	Ri ₀	Re ₀
High Flux	0.004	14.90	58.5	0.15	330
Medium Flux	0.004	8.60	33.7	0.44	190
Low Flux	0.004	2.40	9.4	5.90	55

number and Re₀ is the inlet Reynolds number, defined by the following relations:

$$A = b_o \times h_o, \quad (5)$$

$$Q_0 = U_{in} A, \quad (6)$$

$$B_o = \frac{\Delta \rho}{\rho_w} A U_{ave} g, \quad (7)$$

$$Ri_0 = \frac{\Delta \rho g h_0 \cos \theta}{\rho_w U_{in}^2}, \quad (8)$$

$$Re_0 = \frac{\rho U_{in} h_0}{\mu}, \quad (9)$$

where U_{in} = inlet velocity; A = cross-sectional area of the dense layer; ρ_w = ambient density (water density); ρ = mean local density; $\Delta \rho = \rho - \rho_w$; U_{ave} = mean layer velocity and h_0 = inlet height of the density current.

Height and Width of the Dense Layer

The height and width of the dense layer in the laboratory are identified by the naked eye by its brightness. Figure 4 show laboratory pictures of the salt solution density current, reported by Firoozabadi et al. [13]. As can be seen in Figure 4a, there is a sharp interface between two layers. However, Figure 4b indicates a broader interface and a more diffuse shear layer between the dense layer and clear water.

Therefore, it would be a good idea to define the height and width of the dense layer by using the boundary layer concept. Here, it is assumed that the interface is the place where its concentration is about 1% of the inlet concentration, which is denoted by C_{in} .

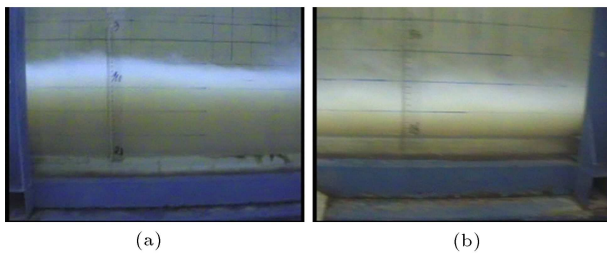


Figure 4. (a) Sharp interface between two layers; (b) Broader interface [13].

In order to non-dimensionalize the velocity and concentration profiles and compare them with the experimental data, the width, denoted by b and the height, denoted by h of the density current are used based on the boundary layer concept.

The stream-wise velocity and concentration profiles at $b/b_o = 7.0$ and $\theta = 10^\circ$ are shown in Figure 5 in comparison with the experimental data of Alavian [10]. A slight underestimation was seen in the velocity and concentration profiles near the interface of the density current and clear water, which can be related to the entrainment at the interface. Based on the authors' assumption, the non-dimensional height of the density current in Figure 5 is $y/h = 1$. Then, one can see that the momentum diffusion in the normal direction (perpendicular to the bed) is larger than that of the concentration.

Depth-Averaged Parameters

Depth-averaged velocity U_{ave} and concentration C_{ave} in a cross-section are calculated with the following equations, using Ellison and Turner [2] concepts, but in 3-D formats:

$$U_{ave} h b = \int_0^{B1} \int_0^{H1} u dy dz, \quad (10)$$

$$U_{ave}^2 h b = \int_0^{B1} \int_0^{H1} u^2 dy dz, \quad (11)$$

$$U_{ave} = \frac{\int_0^{B1} \int_0^{H1} u^2 dy dz}{\int_0^{B1} \int_0^{H1} u dy dz}. \quad (12)$$

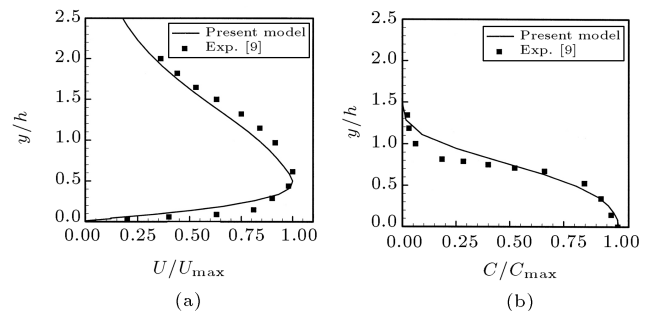


Figure 5. Velocity and concentration profiles at $b/b_o = 7.0$ and $\theta = 10^\circ$, in comparison with Alavian's experiments [10]. (a) Velocity profile; (b) Concentration profile.

Then, the depth-averaged concentration, C_{ave} , in a cross-section is defined by [14]:

$$C_{ave} = \frac{\int_0^{B1} \int_0^{H1} C u dy dz}{\int_0^{B1} \int_0^{H1} u dy dz}. \tag{13}$$

In the above formulas, $H1$ and $B1$ are the height and width of the channel, respectively. Figures 6 and 7 show the variation of U_{ave} and C_{ave} along the channel for medium and high Reynolds numbers at $\theta = 10^\circ$. The figures indicate a considerable rise in U_{ave} and C_{ave} by increasing Re number. In fact, due to the entrainment of fresh water into the dense layer and the conservation of mass, the mean velocity and concentration are expected to decrease in a stream-wise direction as the results show.

Now, by using C_{ave} , U_{ave} and the height of the

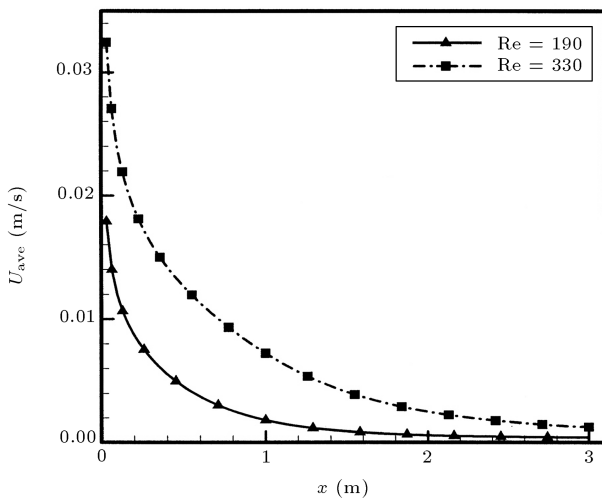


Figure 6. Effects of Re on the U_{ave} .

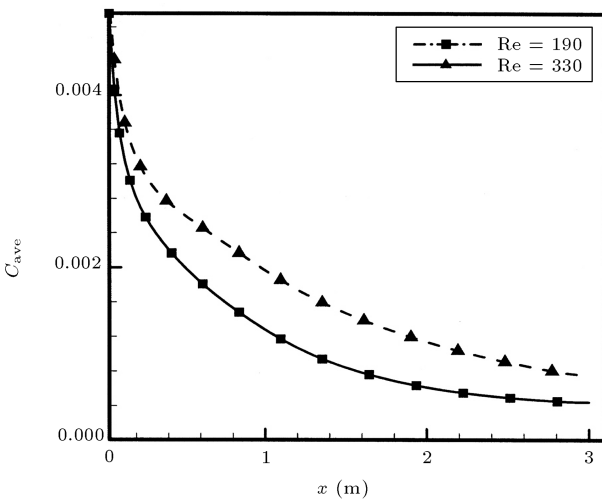


Figure 7. Effects of Re on the C_{ave} .

dense layer (h), Ri_{ave} can be obtained as follows:

$$Ri_{ave} = C_{ave} \frac{\rho_s - \rho_w}{\rho_w} \frac{gh \cos \theta}{U_{ave}^2}. \tag{14}$$

Characteristic Variables

Felix [7] has defined some variables (such as the height of maximum velocity) in natural scale turbidity currents, using a two-dimensional numerical model. Here, the defined height and width of the dense layer are compared based on the boundary layer concept with the depth-averaged parameters and variables defined by Felix [7]. The Felix parameters are maximum velocity U_{max} and multiples thereof ($1/2U_{max}$ and $1/4U_{max}$), layer thicknesses y_{max} (the height of the maximum velocity), $y_{1/2}$ and $y_{1/4}$, which are the heights above maximum velocity, where the velocity is equal to half and one quarter of the maximum velocity, respectively, i.e. the heights being such that $u(y_{1/2}) = 1/2U_{max}$ and $u(y_{1/4}) = 1/4U_{max}$. The concentrations C_m , $C_{1/2}$ and $C_{1/4}$ are calculated from the following:

$$C_m = \frac{1}{y_{max}} \int_0^b \int_0^{y_{max}} C dy dz, \tag{15}$$

$$C_{1/2} = \frac{1}{y_{1/2}} \int_0^b \int_0^{y_{1/2}} C dy dz, \tag{16}$$

$$C_{1/4} = \frac{1}{y_{1/4}} \int_0^b \int_0^{y_{1/4}} C dy dz. \tag{17}$$

Figure 8 indicates the average velocity and height, which are calculated in the present model, and the variables defined by Felix [7] for medium flux and $\theta = 5^\circ$. Felix [7] showed that the height of the dense layer is approximately equal to $y_{1/4}$, but Figure 8a indicates that, in this study, it can be estimated by $y_{1/2}$. This outcome may be due to lateral propagation, which decreases the diffusion of concentration in a y

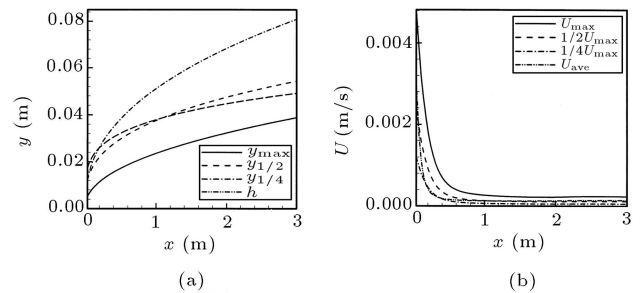


Figure 8. Characteristics and boundary layer height and velocity at medium flux and $\theta = 5^\circ$.

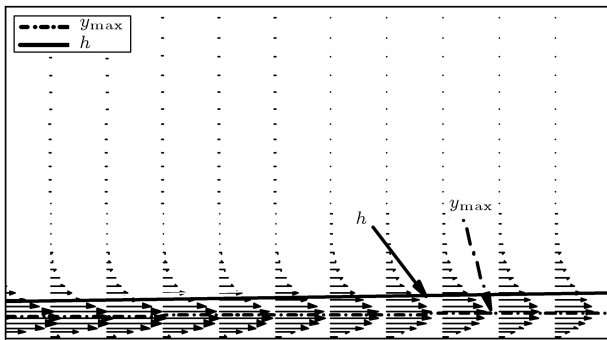


Figure 9. Maximum and boundary layer height and horizontal velocity vector at medium flux and $\theta = 5^\circ$.

direction. Figure 8b shows that the average velocity is, approximately, equal to $1/2U_{max}$, which is the same as the Felix [7] results. Figure 9 shows the height of the dense layer and velocity profiles. As can be seen, the momentum diffusion is larger than that of the concentration and, where concentration reaches 1% C_{in} , the velocity is approximately $1/2U_{max}$.

Lateral Propagation

Figure 10 shows the lateral propagation of the density current and the effects of bed slope and entrance Reynolds number on it. It has been shown that layer width has an inverse relation with bed slope. Lateral spreading decreases as bed slope increases, which is due to the rise of the gravity force component. Hence, it seems that the variations of flux and mean velocity have more effect on lateral spreading than the bed slope. The shape of lateral spreading is also noticeable. In low Reynolds numbers, whose entrance flow rates are low, the dense layer spreads immediately after entering the channel (Figure 10a). But, with increasing flow rate, the dense layer can keep its inertia and spread like a jet without lateral spreading (Figure 10b). In addition, results show that the three-dimensional dense layer approaches a normal state after a considerable distance from the entrance and the flow behaves as a two-dimensional structure.

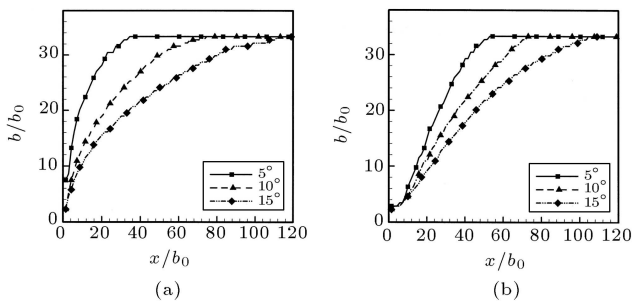


Figure 10. Influence of bed slope on lateral spreading. (a) Low flux; (b) Medium flux.

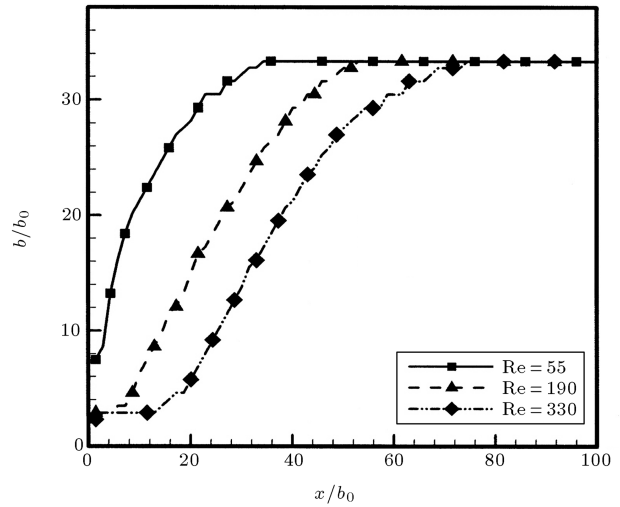


Figure 11. The lateral propagation of 3-D density current at $\theta = 5^\circ$.

Figure 11 shows the influence of increasing flux on lateral spreading at the constant slope. As can be observed, by increasing the flow rate, the inertia becomes more important than the viscous effect and lateral propagation will be retarded.

Figures 12a and 12b show the computed vertical velocity profile of the symmetry plane, which develops on an inclined bed. In these figures, the flow structures are given in dimensionless form, i.e., the vertical axis was non-dimensionalized by the local current height, $h = 0.045$ m, and the horizontal axis by the inlet velocity. Figure 12a shows that, by increasing the distance from the inlet, the maximum velocity value will decrease, due to lateral propagation and inertia decreasing. Also, it is observed that the location of the maximum velocity from the bed will rise, due to mixing and entrainment at the interface. It is also noticeable that, by marching in the x direction, the vertical velocity gradient decreases at the interface, where $y/h = 1.0$ as a reason for entrainment decreasing. Figure 12b indicates the effect of bed slope on the vertical velocity profile. As can be seen, by increasing

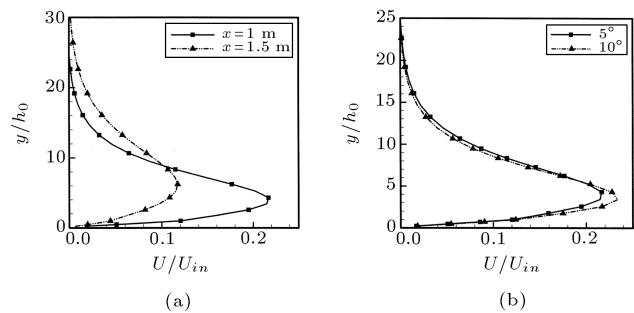


Figure 12. The stream-wise velocity component by (a) Marching in x direction for medium flux and $\theta = 5^\circ$; and (b) The bed slope changing for medium flux and $x = 1$ m.

the bed slope, the maximum velocity value has little increase, due to the gravity force rising. Also, the location of the maximum velocity value will become closer to the bed, as the result of decreasing the dense layer depth.

Figure 13 indicates the variation of concentration profile of the symmetry plane with the bed slope and inflow flux. As can be seen, the effect of the flux on concentration is more important than the slope.

Entrainment

When the advancing front plunges, it disturbs and entrains the surrounding fluid. The upper boundary of the dense layer behaves like a free shear layer. Turbulence at this boundary entrains the stationary ambient fluid immediately above it into the layer and dilutes it. The turbulent region grows with the distance downstream as the non-turbulent fluid becomes entrained in it. This entrainment implies a flow of ambient fluid into the turbulent layer. Therefore, a small mean velocity, perpendicular to the mean flow, is generated along the interface when the ambient fluid is initially at rest. Ellison and Turner [2] suggested that the velocity of the inflow to the turbulent region must be proportional to the velocity scale of the layer; the constant of this proportionality is called the entrainment coefficient, E . Alavian [10] assumed a rectangular cross-section area for a 3-D density current and defined the entrainment coefficient, E , as:

$$\frac{d}{dx}(U_{ave}A) = EU_{ave}(b + 2h), \quad (18)$$

where A is the cross-sectional area of the dense layer. Ellison and Turner [2] showed that a 2-D dense layer following down a sloped bed attains a normal state (established flow), where the overall Richardson number, Ri , reaches a constant value, Ri_n , independent of x . This condition has also been observed in the laboratory investigation of 3-D density currents reported by

Alavian [10], and the following relationship between Ri_n and E was derived:

$$Ri_n = \frac{(\frac{3h}{b} - 1)E - Cd}{(1 + \frac{3}{2}\frac{h}{b})S_2E - S_1tg\theta}. \quad (19)$$

S_1 and S_2 are shape factors, due to the non-uniformity of the density distribution defined, respectively, as [2]:

$$S_1 = \frac{1}{(\Delta\rho/\rho_w)_mh} \int_0^\infty \frac{\Delta\rho}{\rho a} dz, \quad (20)$$

$$S_2 = \frac{2}{(\Delta\rho/\rho_w)_mh^2} \int_0^\infty \frac{\Delta\rho}{\rho a} dz, \quad (21)$$

where $(\Delta\rho/\rho_w)_m$ is the local mean density excess in Table 1. And C_d is the friction coefficient, which is assumed to be constant and can be obtained by [10]:

$$\frac{dh}{dx} = \frac{C_d + (2 - \frac{1}{2}S_2Ri)E - (1 - \frac{1}{2}S_2Ri)\frac{h}{b}\frac{db}{dx} - S_1Ritg\theta}{1 - S_2Ri}. \quad (22)$$

For an established flow away from the source, where $h \ll b$, Equation 19 can be approximated by ignoring h/b compared to unity. Therefore, the normal Richardson number for flow on a steep slope becomes:

$$Ri_n = \frac{C_d + E}{S_1tg\theta - S_2E}. \quad (23)$$

Measuring S_1 and S_2 by Alavian [10] at the dense layer symmetry plane gives $S_1 = 0.35 - 0.84$ and $S_2 = 0.1 - 0.43$. By using the present model, one has the following results: $S_1 = 0.3 - 0.41$ and $S_2 = 0.3 - 0.65$. The drag coefficient, C_d , can be calculated from Equation 22. In this study $C_d = 0.18 - 0.4$, which was found in the range of 0.1-0.2 by Alavian [10].

Figure 14 compares the entrainment coefficient, E , plotted versus the normal Richardson, Equation 8, calculated by [10] with that calculated by the present model. It can be seen that the computations from the present model are in good agreement with the experimental data.

In addition, using this numerical model, the real average Richardson values, without any approximation, can be calculated by Equation 14. Figure 15 indicates that the curve fitted on the results of the present model has the same trend as the curve which fitted on the Turner & Ellison's [2] data for an inclined plume. By increasing the Richardson number, the flow becomes more stable and the entrainment of the clear water to the dense layer decreases. Finally, both curves show the inverse relation between E and Ri . The curve fitted between E and Ri in this study has a linear trend and its relation is given in Equation 24.

$$E = -0.0054Ri + 0.0667. \quad (24)$$

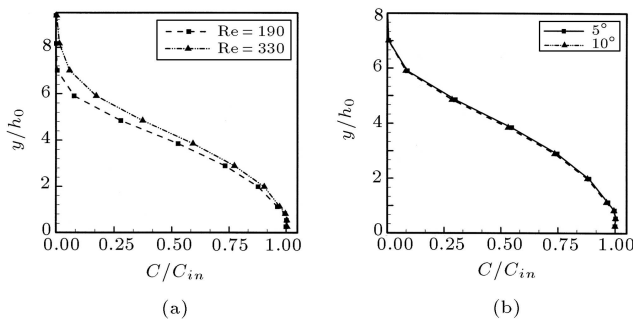


Figure 13. Effects of inlet conditions on the concentration variation. (a) Inflow flux at $\theta = 10^\circ$ and $x = 1.5$ m; (b) The bed slope at high flux and $x = 1.5$ m.

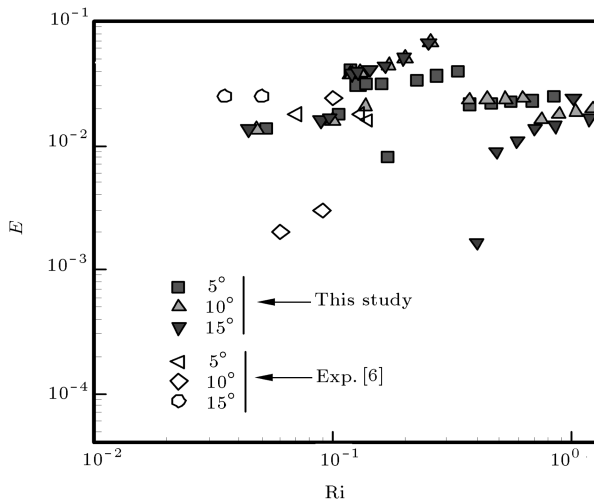


Figure 14. Entrainment coefficient versus normal Richardson number.

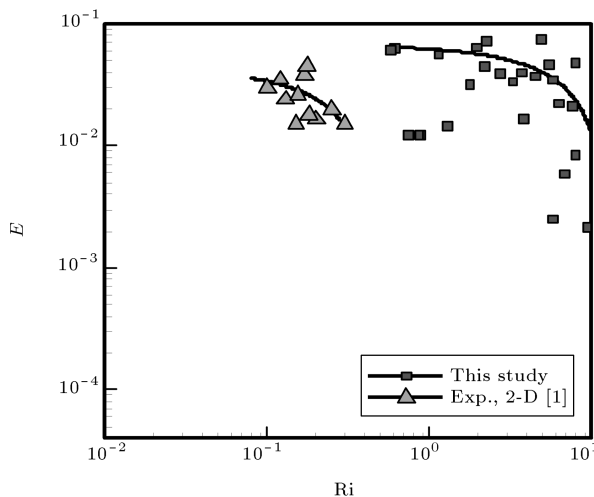


Figure 15. Entrainment coefficient versus average Richardson number.

CONCLUSIONS

In this work, a numerical model is used to simulate a 3-D density current. The viscous analysis is based on three-dimensional Navier-Stokes equations. The equations for mass continuity, momentum conservation and diffusion are solved simultaneously in fixed Cartesian directions, on a non-staggered grid using a finite volume scheme. The velocity-pressure coupling is handled by the SIMPLEC model. Density currents with uniform velocity and concentration enter the channel, via a sluice gate, into a lighter ambient fluid and move forward down the slope on the bed of the channel. The height and width of the current are identified using a boundary layer concept. The outcome height of the density current, which is based on the boundary layer concept, is used to non-dimensionalize the velocity and

concentration profile and the results are in reasonable agreement with the experimental data. A comparison is made between depth-averaged and characteristic variables of a three-dimensional density current, which leads to, $H \approx Y_{\frac{1}{2}}$, $U \approx \frac{1}{2}U_{\max}$ and $C \approx C_{\frac{1}{4}}$. It was found that the flow will reserve its 3-D structure at a considerable distance from the entrance, so it is necessary to study the lateral spreading. This method is capable of determining the span-wise entrainment and propagation of the current, which has been neglected in many previous numerical works. Also, a relation between entrainment coefficients and the Richardson number was obtained without any simplification, which has the same trend as the Ellison and Turner [2] 2-D experimental data.

NOMENCLATURE

h_0	height of sluice gate
b_0	width of sluice gate
C	concentration, $C = (\rho - \rho_w)/(\rho_s - \rho_w)$
g	gravitational acceleration
g'	reduced gravitational acceleration, $g' = g(\rho - \rho_w)/\rho_w$
h	density current depth
b	density current width
P	pressure
Re	Reynolds number, $Re = uh/\nu$
Ri	Richardson number, $Ri = g'h \cos \theta / u^2$
Ri_n	normal Richardson number
u	velocity in x direction
v	velocity in y direction
$U_{\text{ave}}, C_{\text{ave}}$	average value of velocity and concentration
U_{max}	maximum velocity
x	stream-wise coordinates
y	vertical coordinate
λ	molecular diffusion
ρ	density of saline solution
ρ_w	water density
ρ_s	salt density
θ	angle of bed
Q_0	inlet volumetric flux
B_o	buoyancy flux
A	cross sectional area
S_1, S_2	shape factors
C_d	drag coefficient
E	entrainment coefficient
y_{max}	height of maximum velocity

$y_{\frac{1}{2}}$	height above maximum velocity where $u = 0.5U_{\max}$
$y_{\frac{1}{4}}$	height above maximum velocity where $u = 0.25U_{\max}$
C_m	average concentration below y_{\max}
$C_{\frac{1}{2}}$	average concentration below $y_{\frac{1}{2}}$
$C_{\frac{1}{4}}$	average concentration below $y_{\frac{1}{4}}$

REFERENCES

1. Turner, J.S., *Buoyancy Effects in Fluids*, Cambridge University Press, London, UK (1973).
2. Turner, J.S. and Ellison, T. "Turbulent entrainment in stratified flows", *J. Fluid Mech.*, **6**(1), pp 423-448 (1959).
3. Parker, G., Fukushima, Y. and Pantine, H.M. "Self accelerating turbidity currents", *J. Fluid. Mech.*, **171**, pp 145-181 (1986).
4. Garcia, M.H. "Hydraulic jumps in sediment driven bottom currents", *J. Hydraulic Eng.*, **119**(10), pp 1094-1117 (1993).
5. Altinakara, M.S., Graf, W.H. and Hopfinger, E.J. "Flow structure in turbidity currents", *J. Hydraulic Research*, **34**(5), pp 713-718 (1996).
6. Lee, H.-Y. and Yu, W.-S. "Experimental study of reservoir turbidity current", *J. Hydraulic Engineering*, **123**(6), pp 520-528 (1997).
7. Felix, M. "The significance of single value variables in turbidity currents", *J. Hydraulic Research*, **42**(3), pp 323-330 (2004).
8. Ashida, K. and Egashira, S. "Basic study of turbidity currents", *Proc., JSCE*, **237**, pp 37-50 (1975).
9. Bournet, P.E., Dartus, D., Tassin, B. and Vincon-Leite, B. "Numerical investigation on plunging density current", *J. Hydraulic Engineering*, **125**(6), pp 584-594 (1999).
10. Alavian, V. "Behavior of density current on an incline", *J. of Hydraulic Engineering, ASCE*, **112**(1), pp 27-42 (1986).
11. Firoozabadi, B., Farhanieh, B. and Rad, M. "Hydrodynamics of two-dimensional, laminar turbid density currents", *J. of Hydraulic Research*, **41**(6), pp 623-630 (2003).
12. Rhie, C.M. and Chow, W.L. "Numerical study of the turbulent flow past an airfoil with trailing edge separation", *AIAA J.*, **21**, pp 1527-1532 (1983).
13. Firoozabadi, B., Farhanieh, B. and Rad, M. "Hydrodynamics of confined turbidity currents", *Int. J. of Engineering Science*, **12**(4), pp 29-37 (2001).
14. Parker, G., Fukushima, Y. and Pantine, H.M. "Self accelerating turbidity currents", *J. Fluid. Mech.*, **171**, pp 145-181 (1986).